40-GHz photonic waveform generator by linear shaping of four spectral sidebands

Christophe Finot

40-GHz photonic waveform generator by linear shaping of four spectral sidebands

Christophe Finot

Laboratoire Interdisciplinaire Carnot de Bourgogne, UMR 6303, 9 av. Alain Savary, 21078 Dijon, France
christophe.finot@u-bourgogne.fr

Received Month X, XXXX; revised Month X, XXXX; accepted Month X, XXXX; posted Month X, XXXX (Doc. ID XXXXX); published Month X, XXXX

We show that amplitude and phase shaping of only four sidebands of the optical spectrum is sufficient to synthesize parabolic, triangular or flat-top pulse trains at a repetition rate of 40 GHz. Selection of the waveform is easily achieved by changing the phase difference between the inner and outer spectral lines. Experimental results confirm the high quality of the intensity profiles that are obtained.

OCIS Codes: (320.5540) Pulse shaping

Generation of new optical waveforms at repetition rates of several tens of GHz has stimulated a large interest in the photonics community for its applications in all-optical signal processing and microwave signal manipulation. If sinusoidal, Gaussian or hyperbolic secant intensity profiles are now routinely produced by modulators or mode-locked lasers, other profiles such as parabolic, triangular or flat-top pulses remain rather hard to synthesize. Therefore, different strategies have been explored. On the one hand, linear pulse shaping can be used to transform an ultrashort pulse into the desired shape, the transfer function being given in the spectral domain by the ratio of the target field by the input optical field. In this context, linear shaping of picosecond pulses have been achieved by use of spatial light modulators [1, 2], by superstructured fiber Bragg gratings [3], by acousto-optics devices [4] or by an arrayed waveguide grating [5]. On the other hand, several nonlinear approaches have been investigated to take advantage of the progressive evolution of a pulse upon propagation in a normally dispersive fiber : thanks to the Kerr nonlinearity, efficient generation of parabolic intensity profiles [6] or triangular profiles [7, 8] has been demonstrated. Another set of methods is based on the photonic generation relying on the use of specific Mach-Zehnder modulators [9, 10], microwave photonic filters [11] or frequency-to-time conversion [12].

In this contribution, we discuss a new linear approach where the shaping can be done using only two parameters and where it is possible to simply switch from a parabolic pulse to a triangular or flat-top pulse using a single control parameter. Instead of shaping a comb containing tens of spectral components, our target is here to limit our investigation to the minimum number of optical components required to observe the expected shape. If two spectral components only lead to a carrier-suppressed sinusoidal signal, one may wonder if three or four components are sufficient to generate the target waveforms. As we look for a temporal train of symmetric pulses, the optical spectrum is also symmetric, as illustrated in Fig. 1, panels a. For the models based on three or four optical sidebands, only two parameters are therefore required to mathematically describe the optical spectrum. The first parameter is the ratio A between the amplitude of the central components and the amplitude of lateral sidebands. The second parameter is the spectral phase φ of the lateral sidebands relative to the central components.

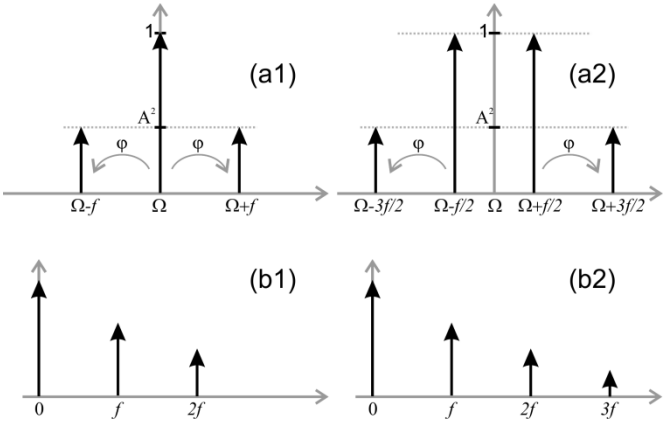

Fig. 1. Optical and RF spectra (panels a and b respectively) of a three and four band model (panels 1 and 2 respectively). Ω is the carrier frequency and f is the repetition rate.

From these spectra, it is relatively easy to retrieve the analytical expressions of the temporal intensity profiles $I_3(t)$ and $I_4(t)$ obtained for the 3 and 4 optical sideband configurations respectively :

$$I_3(t) = 1 + 2A^2 + 4A\cos(\varphi)\cos(\omega_0 t) + 2A^2\cos(2\omega_0 t) \quad (1)$$

$$I_4(t) = 2\left\{\begin{array}{l} 1 + A^2 + \left[1 + 2A\cos(\varphi)\right]\cos(\omega_0 t) + \\ 2A\cos(\varphi)\cos(2\omega_0 t) + A^2\cos(3\omega_0 t) \end{array}\right\} \quad (2)$$

with $\omega_0 = 2\pi f$, f being the repetition rate of the source.

It directly comes from Eq. (1) and (2) that the RF spectra of I_3 and I_4 contain two and three components at non-zero frequencies as illustrated by panels b in Fig. 1. When exploring the space $\{A^2;\varphi\}$, we can make out from Fig. 2(a) that the kurtosis excess calculated over one period of the pulse train may significantly vary : various temporal intensity profiles can be synthesized, with very different levels of flatness as indicated by the positive and negative values of the excess kurtosis. The 4-wave configuration offers a broader range of accessible values.

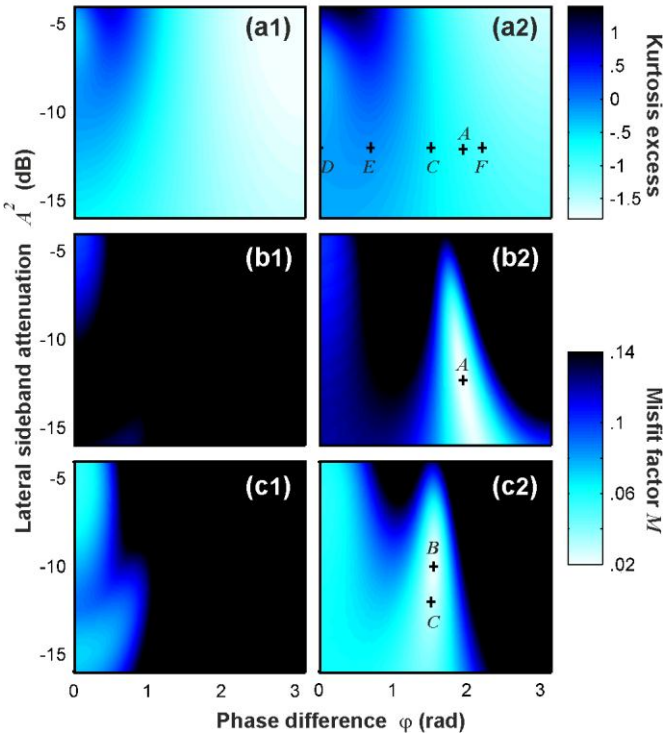

Fig. 2. Evolution of the kurtosis excess (panels a) and of the misfit factor for parabolic and triangular waveforms (panels b and c respectively) according to the phase difference φ and attenuation A^2 of the outer sidebands with respect to the inner sidebands. Results from a three-wave model are compared with results of a four wave configuration (panels 1 and 2 respectively). Points A and B represent the optimum set of parameters for parabolic shapes (used in Fig 3(a)) and for triangular waveforms. Points C, D, E and F are the parameters used in subplots b, c1, c2 and c3 of Fig. 3, respectively.

In order to get more accurate information on the shape that is generated, we have also computed the misfit factor M between the synthesized pulse shape $I(t)$ and a fit by the targeted intensity profile I_{fit} where I_{fit} can be a parabolic or triangular waveform :

$$M^2 = \int \left(I - I_{fit}\right)^2 dt \Big/ \int I^2 \, dt \qquad (3)$$

Results are summarized in the panels (b) and (c) of Fig. 2. Whereas the three component configuration does not allow misfit factors below 0.05, indicating temporal profiles deviating significantly from the target, much lower values are reached for a four band configuration. In this case, a misfit factor as low as 0.018 for parabolic pulses is obtained for parameters $\{A^2;\varphi\}$ being {-12.3 dB;1.95 rad} (point A in Fig 2). Details of the resulting intensity profile at a repetition rate of 40 GHz are given in Fig. 3(a) and demonstrate the very good agreement between the generated profile and the desired shape. However, from the temporal chirp profile, we note that the resulting pulses are far from being transform-limited or linearly chirped. Indeed, contrary to conventional schemes that aim to tailor in the spectral domain both the temporal intensity and phase profiles [1-5], we do not put in our approach any constraint on the temporal phase profile of the target. This is here a crucial point that explains why the number of spectral lines that is required is limited to 4 and that the parameter space to be explored is only bidimensional.

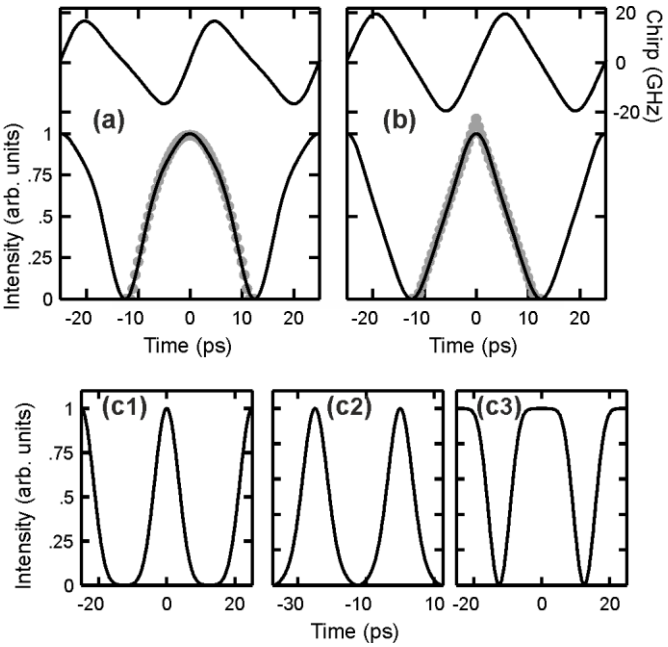

Fig. 3. (a) Temporal intensity and phase profiles obtained for the optimum set of parameters for the generation of parabolic pulse trains (solid black line). The intensity profile is compared with a fit by the desired waveform (solid grey circles). (b) Same as subplot (a) but for triangular pulses with operating parameters corresponding to point C in Fig. 2. (c) Other shapes obtained for an attenuation A^2 of -12 dB and for phase difference φ of 0, 0.70 rad and 2.24 rad : pulsed signal, dark parabolic profile, flat-top pulse (subplots c1,c2 and c3 respectively – see also Media 1). The repetition rate of the pulse train is 40 GHz.

Regarding the triangular waveform, the optimum parameters {-9.9dB;1.55 rad} (point B in Fig 2(c2)) lead to a misfit factor of 0.021. These parameters are consistent with the coefficients of the Fourier series expansion of a full duty-cycle triangular intensity profile: only odd-order harmonics exist and the ratio between the first and third harmonics is 9. Therefore, from Eq. 2, we expect that $A^2 \approx 1/9$ and that the $\cos(\varphi)$ coefficient of the second

harmonics should be close to zero, leading to φ being close to $\pi/2$. However, from the maps of the misfit factors displayed in Fig. 2, it is also worth noting that low misfit factors are found in areas that spread along the vertical direction : for the optimum spectral phase difference φ, a rather good reshaping is achieved with A^2 values that can vary by more than 3 dB. The tolerance on the value of φ is tighter so that it appears that even a relatively small change in the value of φ can enable to switch the waveform from an inverted parabola to a triangle. Keeping the attenuation parameter A^2 equals to -12 dB, we can still retrieve nice triangular shapes for φ = 1.52 rad with misfit factors below 0.03 (point C in Fig 2) and with an excellent linearity of the temporal wings, as outlined in Fig. 3(b). Exploring other phase difference values, we see in Fig 3(c) and in Media 1 that it is possible to obtain other waveforms such as pulses with a duty cycle of 0.32 (defined as the ratio of the full-width at half maximum by the period) when spectral components are in phase (point D in Fig 2). When the φ = 0.70 rad (point E in Fig 2), a train of dark parabolas is generated and for φ = 2.24 rad (point F in Fig 2), a flat-top pulse is obtained with a plateau spanning over 8 ps (the plateau is here defined as the region where the intensity deviates from less than 1% of the peak power). A common feature of all those waveforms that is intrinsically linked to our method with a limited degree of complexity is that we only generate here a given shape without any flexibility on parameters such as the duty cycle: contrary to more evolved methods based on full spectral shaping of a comb or on nonlinear tailoring, it is not possible to change the temporal duration of the structures at a given repetition rate.

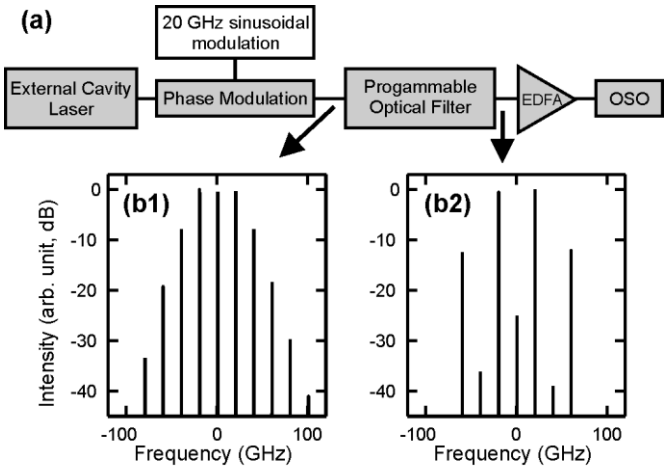

Fig. 4. (a) Experimental setup : EDFA – Erbium Doped Fiber Amplifier ; OSO – Optical Sampling Oscilloscope. (b) Optical spectrum after the phase modulator (b1) and after the programmable optical filter (b2). Frequencies of the optical spectra are relative to the carrier frequency (192.70 THz).

In order to experimentally validate the feasibility of our approach at a repetition rate f of 40 GHz, we have implemented the setup depicted in Fig. 4(a) and made from commercially available components operating at telecommunication wavelengths. A continuous-wave laser (an external-cavity laser) is first phase modulated using a Niobate-Lithium modulator electrically driven by a 20-GHz sinusoidal signal. The resulting spectrum recorded on a high resolution optical spectrum analyzer is plotted in Fig. 4(b1) and clearly exhibits a spectrum made of components separated by 20 GHz and having a central spectral line. This expanded spectrum is then spectrally shaped by a liquid crystal on silicon programmable optical filter (Finisar Waveshaper) in order to achieve simultaneously several operations [2]. First, the central and all the even components are removed to get a carrier suppressed signal at a repetition rate that is doubled. The extinction by 23 dB of those unwanted components therefore enables to optically generate a 40 GHz pulse train starting from a 20 GHz electrical clock [13]. Then, only four components are kept and the components at $\pm f / 2$ are attenuated in order to reach a ratio A^2 of 12 dB between the inner and the outer sidebands. At the same time, the programmable optical filter imprints the phase difference between the various spectral components. The resulting spectral profile shown in Fig. 4(b2) is fully symmetric and is in agreement with the spectrum on which we have based our discussion. At the output, the signal is amplified and detection with an optical sampling oscilloscope (OSO) with a time resolution of 1 ps enables us to get access to the details of the temporal intensity profile.

Results of the temporal characterization are given in Fig. 5 and demonstrate the generation of the expected pulse shapes at a repetition rate of 40 GHz. High-quality parabolic profiles are successfully achieved (Fig. 5(a)). If we decrease by 0.42 rad the value of φ without changing A, a close-to-ideal triangular profile is obtained (Fig. 5(b)). On the contrary, when increasing φ by 0.26 rad, a train of flattened pulses is observed (Fig. 5(c)). This is fully consistent with our previous discussion and confirms that, for an appropriate level of attenuation, changing φ is sufficient to switch from one pulse shape to the other one. From the OSO recordings, we can also make out the relatively low levels of amplitude and timing jitter of the pulse train. Switching between the waveforms requires only a few seconds. The experiment has also been proven to be very stable and has been running for days without noticeable degradation of the performances.

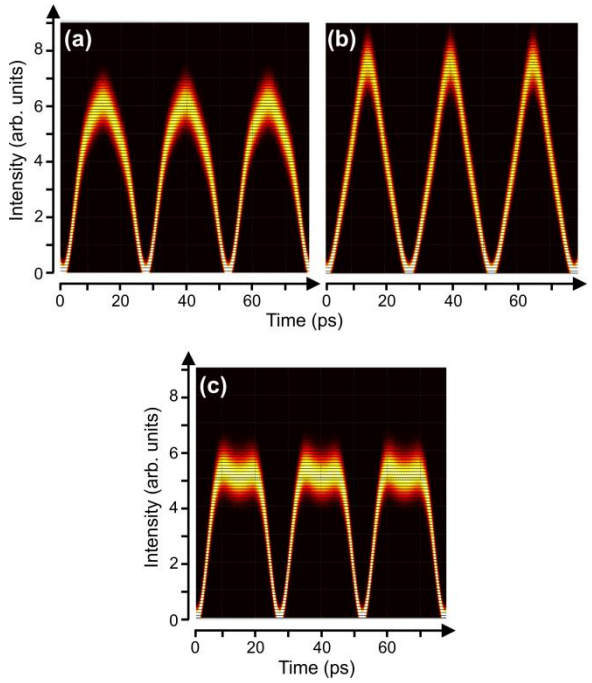

Fig. 5. Temporal intensity profiles recorded on the optical sampling oscilloscope for the parabolic, triangular and flat-top pulse trains (subplots (a), (b) and (c) respectively).

To conclude, we have shown that in order to obtain parabolic or triangular waveforms, amplitude and phase shaping of three spectral sidebands was not accurate enough. By relaxing the constraints on the temporal duration and phase profile, four spectral sidebands are sufficient, which reduces the choice of the physical parameters to a bidimensional problem. When the attenuation ratio between central and lateral spectral lines is conveniently chosen, selection of the waveform is easily achieved by changing the phase difference between the components and other pulse shapes can be generated such as flattened profiles or inverted parabolas. The efficiency of our simple and cost-effective photonic waveform generator is experimentally validated by the high quality of the full duty-cycle intensity profiles that are recorded at 40 GHz.

With the advent of 40 GHz phase modulators, the principle of our approach can be directly extended to the generation of simple symmetric waveforms at a repetition rate up to 80 GHz. Moreover, microresonator-based generation of stable coherent combs with frequency spacing above 100 GHz [14] paves the way for simple and efficient ultra-high repetition rate generation of advanced pulse shapes. In our proof-of-principle demonstration, a programmable optical filter has been involved but we can also imagine replacing this component by an association of less expensive components suitable for operation at other wavelengths. Indeed, using a phase modulator driven by a properly chosen amplitude could enable to directly obtain the good ratio between the spectral components. Suppression of half of the spectral lines can then be done by a simple interferometric device with a convenient free spectral range. Finally, the phase difference between the inner and outer spectral components can be imprinted by a compact dispersive element such as a chirped fiber Bragg grating. Another possibility for the first stages could be to use a single-drive Mach-Zehnder modulator biased at its minimum transmission point [9].

We acknowledge the financial support of the Conseil Regional de Bourgogne (Pari Photcom) and the funding of the Labex ACTION program (ANR-11-LABX-01-01). The experimental work has benefited from the PICASSO Platform of the University of Burgundy.

References.

1. S. T. Cundiff and A. M. Weiner, Nat. Photonics 4, 760-766 (2010).
2. A. M. Clarke, D. G. Williams, M. A. F. Roelens, and B. J. Eggleton, J. Lightw. Technol. 28, 97-103 (2010).
3. F. Parmigiani, P. Petropoulos, M. Ibsen, and D. J. Richardson, IEEE Photon. Technol. Lett. 18, 829-831 (2006).
4. E. R. Andresen, J. M. Dudley, C. Finot, D. Oron, and H. Rigneault, Opt. Lett. 36, 707-709 (2011).
5. T. Hirooka, M. Nakazawa, and K. Okamoto, Opt. Lett. 33, 1102-1104 (2008).
6. C. Finot, J. Fatome, S. Pitois, and G. Millot, IEEE Photon. Technol. Lett. 19, 1711-1713 (2007).
7. S. Boscolo, A. I. Latkin, and S. K. Turitsyn, IEEE J. Quantum Electron. 44, 1196-1203 (2008).
8. B. G. Bale, S. Boscolo, K. Hammani, and C. Finot, J. Opt. Soc. Am. B 28, 2059-2065 (2011).
9. L. Jing, N. Tigang, P. Li, J. Wei, Y. Haidong, C. Hongyao, and Z. Chan, IEEE Photon. Technol. Lett. 25, 952-954 (2013).
10. F. Zhang, X. Ge, and S. Pan, Opt. Lett. 38, 4491-4493 (2013).
11. W. Li, W. T. Wang, W. H. Sun, W. Y. Wang, and N. H. Zhu, Opt. Express 22, 14993-15001 (2014).
12. J. Ye, L. Yan, W. Pan, B. Luo, X. Zou, A. Yi, and S. Yao, Opt. Lett. 36, 1458-1460 (2011).
13. D. K. Serkland, G. D. Bartolini, W. L. Kath, P. Kumar, and A. V. Sahakian, J. Lightw. Technol. 16, 670-677 (1998).
14. F. Ferdous, H. Miao, D. E. Leaird, K. Srinivasan, J. Wang, L. Chen, L. T. Varghese, and A. M. Weiner, Nat. Photonics 5, 770-776 (2011).